Optical Study of Two-Dimensional InP-Based Photonic Crystals by Internal Light Source Technique

Rolando Ferrini, David Leuenberger, Mikaël Mulot, Min Qiu, *Associate Member, IEEE*, Jürgen Moosburger, Martin Kamp, Alfred Forchel, Srinivasan Anand, and Romuald Houdré

***Abstract*—We present the first optical study of 2-D photonic crystals (PCs) deeply etched in an InP/GaInAsP step-index waveguide. Following the same internal light source approach proposed by Labilloy and coworkers for the investigation of GaAs-based 2-D PCs, transmission measurements through simple PC slabs and 1-D Fabry–Pérot (FP) cavities between PC mirrors were performed. Details are given on the experimental setup which has been implemented with respect to the original scheme and adapted to InP-based systems working at 1.5-μm. 2-D plane-wave expansion and finite difference time-domain (FDTD) methods are used to fit the experimental data. Out-of-plane losses were evaluated according to a recently introduced phenomenological model. In spite of the complex hole morphology in the measured samples, preliminary results are presented which indicate the possibility of separating different loss contributions from finite etch depth and hole shape. As for 1-D cavities, both FDTD and classical theory for planar resonators are applied in order to deduce the optical properties of the PC mirrors. The origin of an anomalously high transmission observed inside the stopgap is discussed and arguments are given to demonstrate the need for further modeling efforts when working in the bandgap regime.**

***Index Terms*—Chemically assisted ion beam etching, Fabry–Pérot resonators, finite difference time-domain modeling, GaInAsP/InP, integrated optics, internal light source experiments, luminescence, photonic crystals, plane-wave expansion method, radiation losses, semiconductor heterostructures.**

I. Introduction

PHOTONIC crystals (PCs) consist of periodic arrangements of dielectric (or metallic) elements with a strong dielectric contrast [1]. In these structures, the achieved wavelength-scale periodicity affects the properties of photons in a way similar to that in which semiconductor crystals affect the properties of electrons. Light propagation along particular directions is forbidden within relatively large energy bands known as *photonic bandgaps* (PBGs) [2] in analogy with the concept of electronic bandgap in semiconductors. Initially proposed as a generalization of 1-D dielectric Bragg mirrors to two or three directions [2], [3], PCs have opened new ways to tailor the light–matter interaction and in particular to control spontaneous emission [2], [4]. Moreover, the introduction of line or point defects into simple PCs results into allowed photonic states inside the stopgap, whose shapes and properties are dictated by the nature of the defect, e.g., guided modes propagating in a line defect or cavity modes confined in a point defect. These promising capabilities of PCs have led to the design of new photonic systems with potentially superior properties for photon confinement [5].

Among the large variety of PCs, of particular interest are three-dimensional (3-D) PCs. Since their bandstructure can present a complete PBG, from the basic physics point of view, 3-D PCs are the ideal structures for light control. Up to now, their study and their effective application in optical devices have been strongly limited by complex fabrication problems. Many fabrication techniques have been investigated in order to achieve 3-D semiconductor-based structures both at optical and at infrared wavelengths [6]–[10]. However, in many cases, reproducibility, reliability, control of PC parameters, application to real devices, etc., are still open issues and their fabrication is still a grand challenge.

On the other hand, it has been proven that, although an omnidirectional PBG is only possible in 3-D PCs, a 2-D PC combined with a step-index waveguide in the vertical direction offers enough light control for integrated optics applications [11]. Up to now, the potentials of this approach has been successfully demonstrated in GaAs-based structures, for wavelengths ranging from 900 to 1100 nm [12]–[16]. First, concerning future applications in photonic integrated circuits, remarkable advantages stem from the use of mature fabrication technologies, such as standard epitaxy, e-beam, and nanolithography techniques [17]. Furthermore, the vertical guiding structure combined with an internal light source (ILS) allows the optical characterization of PCs. Photoluminescence (PL) emission is excited inside the heterostructure through which the PC is etched and then guided toward the PC itself [13], [14]. Finally, 2-D PCs deeply etched in *low* refractive index contrast slab waveguides have been demonstrated to be the preferable approach to reduce out-of-plane losses in compact PC structures with many close-packed defects [18], [19].

In the last few years, the use of 2-D or quasi-2-D PCs has been widely explored in order to improve the overall performances of optoelectronic devices [5], [20]. In particular,

Manuscript received September 18, 2001; revised March 11, 2002. This work was supported by the European Union through the IST Project PCIC under Contract 1999-11239.

R. Ferrini, D. Leuenberger, and R. Houdré are with the Institut de Photonique et d'Electronique Quantique, Ecole Polytechnique Fédérale de Lausanne, CH-1015 Lausanne, Switzerland (e-mail: ferrini@dpmail.epfl.ch).

M. Mulot, M. Qiu, and S. Anand are with the Department of Microelectronics and Information Technology, Royal Institute of Technology (KTH), S-16440 Kista, Sweden.

J. Moosburger, M. Kamp, and A. Forchel are with the Technische Physik, University of Würzburg, D-97074, Würzburg, Germany.

Publisher Item Identifier S 0018-9197(02)05715-9.

0018-9197/02$17.00 © 2002 IEEE

the possibility of exploiting the capabilities of PC-based photonic integrated circuits in multichannel wavelength-division multiplexing devices has been envisaged [21]. Since InP is the material system most commonly used in long-wavelength telecommunications applications, InP-based PCs have been studied, such as GaInAsP/InP 2-D PCs formed by submicrometer column arrays [22], [23]. Two-dimensional PC mirrors have been used in InP-based short cavity lasers [24], while many efforts have been devoted to fully PC-based emitters, like membrane-based PC defect lasers [25]–[27] or PC cavity lasers fabricated in air/GaInAsP/SiO_2/Si [28] and air/GaInAsP/Al_2O_3 [29] vertical step-index waveguides. Also, passive structures have been realized by etching PC-based waveguides into a GaInAsP film cladded between air and SiO_2 [30]. In spite of this remarkable progress, due to the use of *high* index contrast heterostructures, the performance of these devices is strongly affected by out-of-plane losses [18], [19]. Moreover, although *low* contrast slab waveguides have proved so promising in GaAs-based applications, this approach was still lacking in InP-based systems.

In this paper, we present the first optical study of quasi-2-D PCs with *low* vertical light confinement fabricated into an InP/GaInAsP slab waveguide containing GaInAsP quantum wells (QWs) as a built-in probe source. PC structures consisting of a triangular lattice of air holes have been etched normally to the guide plane. Based on the results obtained in GaAs-based systems [12], moderate air-filling factor values ($f \sim 0.30$) and air hole diameters have been chosen to minimize out-of-plane losses. Such low f values result in a full gap only in the transverse electric (TE) polarization direction. The ILS approach originally proposed for the investigation of GaAs-based 2-D PCs [12] was exploited to characterize the optical properties of the fabricated PC structures. The original setup was implemented and adapted to InP-based systems working in the integrated optics spectral window around 1.5 μm. In Section II, the ILS experimental principle is briefly described. In Section II-A, details of the experimental setup are illustrated, while Sections II-B and II-C describe the experiments performed on simple PC slabs and on 1-D Fabry–Pérot (FP) cavities, respectively. In Section III-A, the main structural and optical properties of the GaInAsP/InP heterostructure are discussed. PC fabrication is presented in Section III-B, where details of both the e-beam and on the etching procedures are given. Also, the main results of the PC structural characterization are shown. In Section III-C the layouts of PC slabs and 1-D cavities are briefly sketched. The properties of the probe beam are illustrated in Section IV-A, where the emission from the GaInAsP QWs is analyzed in detail. In particular, the QW reabsorption effects on the spectral shape of the guided beam are discussed and the choice of GaInAsP QWs as the source is substantiated. Section IV-B is devoted to the experimental results on simple PC slabs. Transmission spectra are shown and compared to theory. Two-dimensional plane-wave expansion (PWE) and finite difference time-domain (FDTD) methods are used to best-fit the experimental data. The results of the FDTD best-fit are analyzed in the framework of the out-of-plane loss model proposed in [18]. In order to reproduce the complex hole morphology in the measured samples, the

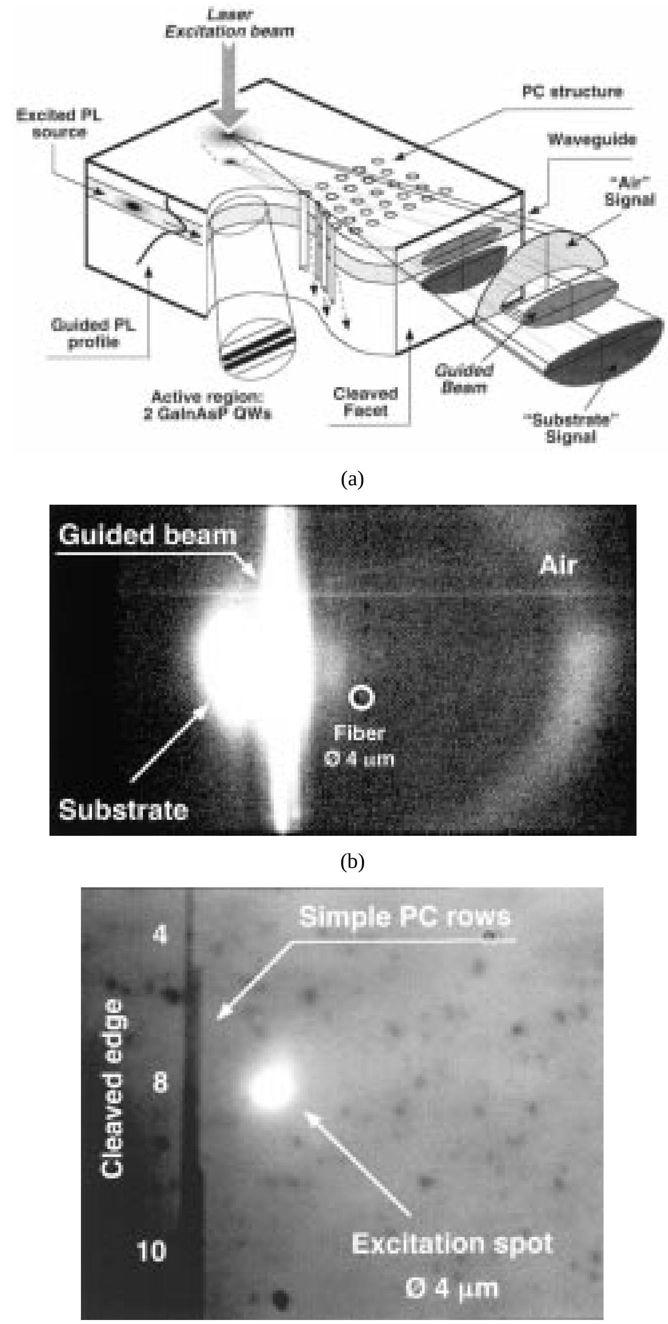

(a)

(b)

(c)

Fig. 1. (a) General experimental configuration for ILS measurements. PL emission is excited inside two GaInAsP QWs (active region) embedded in a InP/GaInAsP slab waveguide and then guided toward the PC structure. Dashed arrows indicate out-of-plane losses toward the substrate. The three beams escaping from the cleaved facet after propagation through air, substrate, and inside the guide are sketched. (b) Typical image of the three signals when the collection optics focal plane coincides with the cleaved facet. The white circle ($\oslash = 4\ \mu$m) represents the conjugate image of the collection fiber. (c) Front image of a ΓM-oriented simple PC slab consisting of three blocks of 4, 8, and 10 air hole rows, respectively. The arrow shows the typical excitation spot ($\oslash = 4\ \mu$m).

ideal cylindrical hole shape was substituted by a more realistic cylindro–conical shape. Preliminary results are shown which reveal the possibility of separating loss contributions from hole depth and shape. Predictions are made on further fabrication improvements needed to reduce losses in the allowed bands for

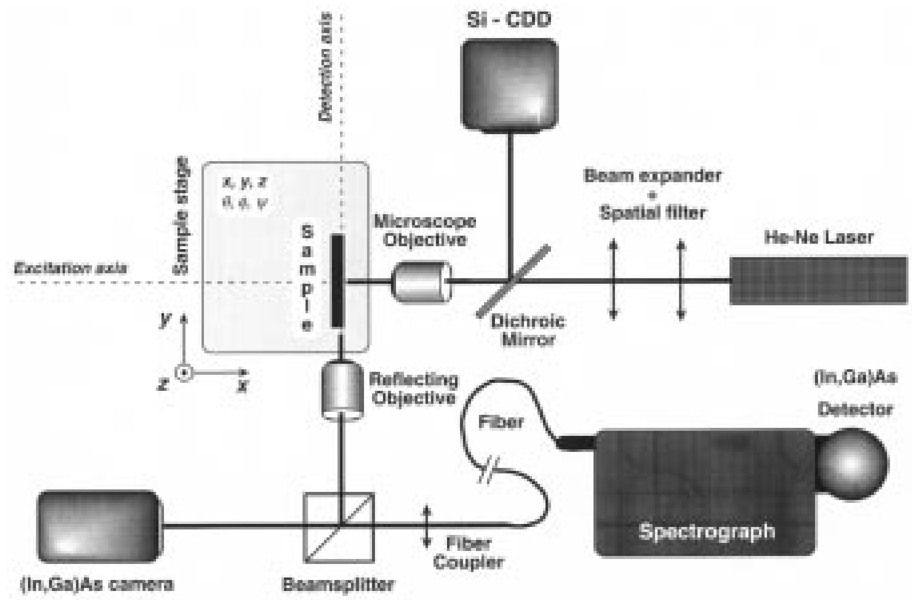

Fig. 2. Scheme of the ILS experimental setup.

light propagation. In Section IV-C transmission spectra through 1-D FP cavities are presented and the optical properties of the PC mirrors are indirectly obtained studying the FP resonances inside the PBG. An anomalously high transmission inside the stopgap is demonstrated and discussed.

II. Internal Light Source Technique

In the last few years, the ILS technique has been successfully applied to the study of quasi-2-D PC structures deeply etched in GaAs-based vertical step-index waveguides [12]. This method has been demonstrated to be a powerful tool both to assess some fundamental PC properties and to measure reflection (R), transmission (T), and diffraction [13]–[16], eliminating difficulties and uncertainties arising in standard optical techniques (e.g., the "end-fire" method [31]–[35]).

A. Experimental Setup

In Fig. 1(a), the general configuration for ILS experiments is illustrated. The PL excited inside two GaInAsP QWs embedded in an InP/GaInAsP slab waveguide is used as a built-in light source. Part of the PL signal propagates parallel to the surface as a guided mode and interacts with the PC structure. Then, the image of the guided beam escaping from the sample through a cleaved facet is coupled into a multimode optical fiber ($\phi = 100$ μm) for spectral analysis. Due to refraction at the layer boundaries, three different beams come out from the cleaved facet after propagation through air, substrate, and inside the guide, respectively [see Fig. 1(a)]. As discussed in [13], when the distance d between the excitation spot and the edge is large enough (e.g., $d > 30$ μm), the cross-talk between the three signals is negligible and the selective analysis of the guided light can be performed by imaging the edge signal. Fig. 1(b) shows a typical image obtained when the collection optics is focused on the facet. The guided beam appears as a focused bright line along the edge while the white circle ($\phi' = 4$ μm) represents the conjugate image of the collection fiber. The guided contribution can be selected and spatially resolved aligning the circle with the bright line.

A detailed scheme of the experimental setup is shown in Fig. 2. A setup similar to the one used to investigate GaAs-based 2-D PCs ($\lambda = 1$ μm) in [12]–[14] was modified to perform ILS experiments also on InP-based systems ($\lambda = 1.5$ μm). A 10-mW He–Ne laser ($\lambda = 633$ nm) is used to excite spontaneous emission inside the GaInAsP double-QW active region. The laser beam is expanded and spatially filtered. A 40$\times$ microscope objective with numerical aperture NA $=$ 0.65 focuses the beam onto the sample surface. The achieved excitation spot diameter $\oslash = 4$ μm yields a maximum pumping density of 50 kWcm^{-2}. When focusing the laser beam, the use of a dichroic mirror along with an Si-CCD camera supplies the simultaneous imaging of the sample front surface and the excited PL spot [see Fig. 1(c)]. The light beams escaping from the cleaved facet are collected with a perfectly achromatic 36$\times$ Cassegrain objective. The limited numerical aperture (NA $= 0.5$) gives an internal in-plane collection angle $\theta < 9^\circ$ and assures the directionality of the measurement [13]. A polarizer allows one to select the TE-polarized component of the signal. Finally, as mentioned above, a beamsplitter is used to split the collected signal into two beams. The first is focused by a long-focal lens onto an (In, Ga)As near-infrared area camera to image the facet signal. The second beam is coupled into the fiber and fed into a 0.46-m flat-field imaging spectrograph for spectral analysis. The spectrometer is equipped with a 150-lines/mm grating blazed at 1200 nm (resolution $=$ 1 nm/pixel; total covered spectral range $=$ 360 nm) and a liquid N_2 cooled (In, Ga)As photon counting array detector.

B. Experiments on PC Slabs

The experimental configuration for PC slab transmission measurements is illustrated in Fig. 3(a). The reference signal $I_1(\lambda)$ and the PC-related signal $I_2(\lambda)$ are measured keeping

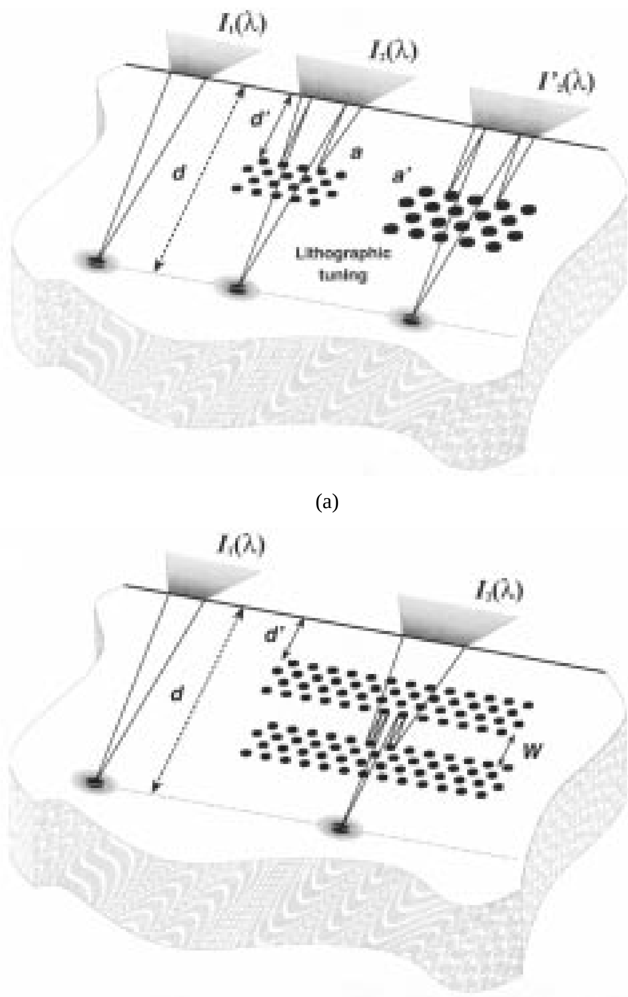

(a)

(b)

Fig. 3. (a) Experimental configuration for PC transmission measurements. The distances between the edge and both PC slabs (d') and the excitation spot (d) are kept constant. The reference $I_1(\lambda)$ is taken in an unetched area and $I_2(\lambda)$ spectra are collected from PC slabs with different periods (lithographic tuning). (b) The same configuration is applied to 1-D FP cavities: FP resonances appear in the collected spectra at different energies according to the spacing W between the PC mirrors.

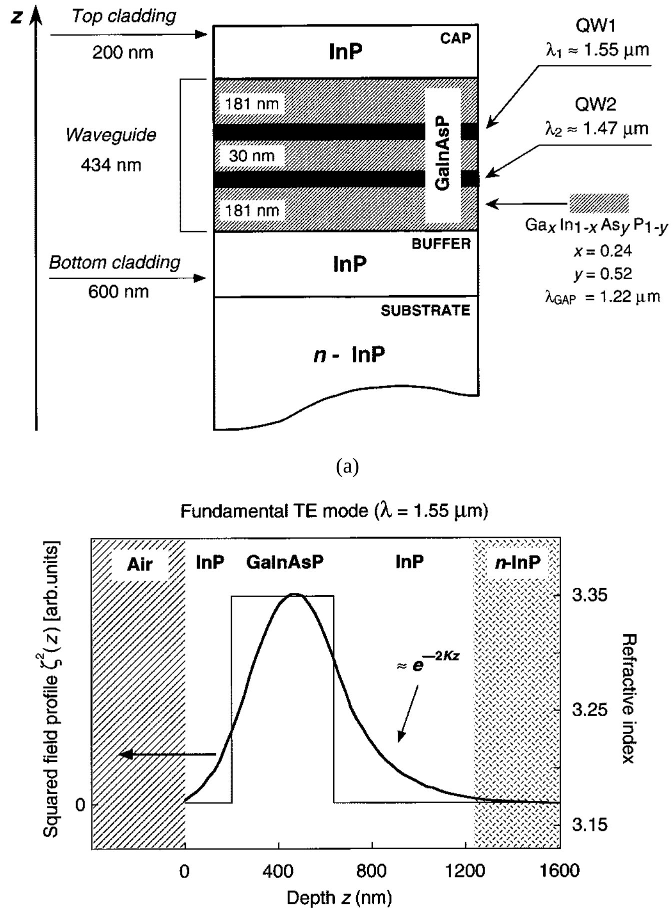

(a)

(b)

Fig. 4. (a) InP/GaInAsP waveguide heterostructure. Two strain-compensated GaInAsP QWs (QW1 and QW2) emitting at two different near-infrared wavelengths (λ_1 and λ_2) are embedded in the GaInAsP guide layer. (b) Refractive index profile of the InP–GaInAsP/InP step-index waveguide. The calculated squared field profile $\zeta^2(z)$ of the fundamental TE mode ($\lambda = 1.55\ \mu$m) propagating inside the guide core is shown. The exponential decay ($\approx \exp(-2Kz)$) of the mode in the lower cladding layer is also evidenced.

constant the distance d between the excitation points and the cleaved facet. High d values ($d \geq 60\ \mu$m) are generally chosen to selectively detect only the vertical guide fundamental mode (see Section III-A). Provided that the PL emission remains homogenous, the ratio $I_2(\lambda)/I_1(\lambda)$ yields the absolute transmission spectrum $T(\lambda)$ of the PC slab. Due to the limited width ($\Delta\lambda \sim 100$ nm) of the probed spectral range, "lithographic tuning" [12] is used. Instead of fabricating several samples with appropriately tuned active layers, the QW emission wavelength is kept constant and the scaling property of PCs [1] is exploited. PC slabs with different pitch (a) values and constant air filling factor (f) are measured and the whole PBG is explored as a function of the reduced frequency $u = a/\lambda$.

C. Experiments on 1-D FP Cavities

The deduction of R data from the PC slab $T(\lambda)$ spectra is not straightforward and the obtained values are strongly affected by experimental uncertainties [14]. Nevertheless, it is well known that the extraction of high R values from measurements on high finesse planar 1-D FP cavities is a more accurate technique [37]. As shown in Fig. 3(b), such cavities can be easily created by introducing a spacer (i.e., a line defect) between two PC slabs etched parallel to the cleaved edge [36], [38]. Single slab optical properties can be accurately deduced from the analysis of the FP resonance peaks appearing in the transmission spectrum [39]. In particular, quality factor Q (or finesse F) and peak transmission ($T_{\max}$) values are function of single mirror T and R values.

III. Sample Details

A. GaInAsP/InP Heterostructure

Details on the GaInAsP/InP heterostructures are shown in Fig. 4(a). They were grown by metal–organic vapor phase epitaxy on n-InP substrates. The heterostructure is nominally undoped and consists of a InP/$Ga_xIn_{1-x}As_yP_{1-y}$/InP waveguide with a built-in light source. The waveguide core is a $Ga_{0.24}In_{0.76}As_{0.52}P_{0.48}$ layer lattice matched to InP and with a direct bandgap emission wavelength $\lambda_{GAP} = 1.22\ \mu$m. The light source consists of two $Ga_xIn_{1-x}As_yP_{1-y}$ strain-compensated QW packages (QW1 and QW2) separated by a

30-nm spacer and located approximately in the middle of the guiding structure between two 181-nm-thick barrier layers. The composition and thickness of the wells were optimized to obtain emission wavelengths $\lambda_1 \sim 1.55$ μm and $\lambda_2 \sim 1.47$ μm for QW1 and QW2, respectively. The total thickness of the guide layer, including the QWs, is 434 nm. The cladding of the waveguide was achieved sandwiching the core between a 200-nm-thick InP cap layer (top) and a 600-nm-thick InP buffer layer (bottom).

The refractive index profile of the InP/GaInAsP/InP waveguide is shown in Fig. 4(b). In the spectral region of interest (i.e., $\lambda = 1.55$ μm), the values $n_{\rm core} = 3.35$ and $n_{\rm clad} = 3.17$ were assumed for GaInAsP and InP, respectively. The resulting structure is a multimode waveguide with three propagating TE modes [40]. The effective refractive index corresponding to the fundamental TE mode was calculated yielding the value $n_{\rm eff}$(calc) $=$ 3.23. The squared field profile $\zeta^2(z)$ of the mode is presented in Fig. 4(b); its maximum is slightly shifted from the center of the core layer, while it decays exponentially in the cladding layers. The shift between the profile peak and the location of the QWs slightly reduces the QW reabsorption on the propagating mode. We note that, due to the material dispersion, $n_{\rm eff}$ is a function of λ and, for a PL beam centered at $\lambda = 1500$ nm (see Section II-B and Fig. 9), the effective index dispersion of the guided mode is $\partial n/\partial\lambda = -2.5 \times 10^{-4}$ nm^{-1} [39]. Then, since for a single ILS measurement a spectral interval $\Delta\lambda \sim 100$ nm is probed and $\Delta n = \Delta\lambda \times (\partial n/\partial\lambda)$, dispersion-corrected $n_{\rm eff}$ values are found to range from 3.23 to 3.255. In order to average the effect of dispersion on the guided mode, the value $n_{\rm eff} = 3.24$ was assumed for the calculations discussed in Section IV. Concerning the two higher order TE modes traveling in the waveguide, they are found to lie mostly in the cladding layers. As mentioned in Section II-B, for propagation distances longer than 60 μm, they leak completely into the substrate and the probe light is in the fundamental mode.

B. PC Structure Fabrication

PC structures were etched in the GaInAsP/InP heterostructures by e-beam lithography and chemically assisted ion beam etching (CAIBE). Two samples were fabricated with $a =$ 240–500 nm ($\Delta a = 20$ nm) and different intended f values: $0.25 < f < 0.30$ for sample A, and $0.30 < f < 0.35$ for sample B. Details of the PC layouts will be given in Section III-C.

In order to form a durable etch mask for the subsequent CAIBE process used to fabricate the PCs in the semiconductor heterostructure, the procedure already described in [24] for InP-based systems was adopted. A value of 150 nm of SiO_2 was sputtered on the sample yielding an etch mask suitable for high-resolution patterning. The triangular PC pattern was written in 500-nm spin coated polymethylmethacrylate (PMMA) resist by e-beam exposure. Details on the standard e-beam procedure are given in [41]. After development of the PMMA in 1 : 3 methylisobutylketone/propanol, the PC hole pattern was transferred into the SiO_2 layer using CHF_3/Ar-based reactive ion etching (RIE). We remark that this two-step writing method provides higher selectivity in the mask patterning, while the use of thicker masks allows one to achieve deeper holes.

In PC structures made of air holes deeply etched into semiconductor heterostructures, losses strongly depend on the hole morphology [42]–[44]. We are reminded that an insufficient hole depth with respect to the vertical extent of the mode field profile [43] and/or a conical hole shape [44] increase light scattering into the substrate (see Section IV-B). Thus, in order to minimize out-of-plane losses, the etching procedure has to provide deep holes ($>$1.5 μm) with as vertical/straight walls as possible. This requires an etch process supplying high anisotropy and high aspect ratios. In the case of microstructures, it has been shown that CAIBE based on Ar/Cl_2 can be used to obtain vertical profiles with high aspect ratio [45]. Moreover, in a previous work [46], the advantages of this procedure for PC etching have been shown in comparison to the standard methane-based RIE. Thus, Ar/Cl_2 CAIBE was applied to etch PC structures into InP/GaInAsP slab waveguides using the e-beam exposed SiO_2 masks. In Ar/Cl_2 ion beam eatching, the sample is sputtered by an energetic argon ion beam with 5 sccm flow and 400 eV ion energy. At the same time chemical attack is generated by a 1-sccm chlorine flow. Bombarding argon ions preferentially sputters phosphorus atoms whereas chlorine enhances the removal of indium atoms by reacting with them to form volatile etch products ($InCl_x$). However, the vapor pressure of $InCl_x$ etch products is quite low at room temperature. Consequently, the sample needs to be heated to obtain efficient removal of $InCl_x$. The hole morphology was found to be optimal at a temperature of about 220 °C and for an etch interval of 20 min.

Fig. 5 shows (a) the cross section and (b) the top-view scanning electron micrographs (SEMs) of a PC test structure with the same f value as sample A and $a = 400$ nm. The hole shape is conical with nearly vertical walls close to the surface and a strongly tapered bottom. The hole morphology is similar for all f and a values. The measured dependence of the hole depth on a is presented in Fig. 6 for both samples. In the inset, the hole depth versus the nominal hole diameter D is shown: similar curves were obtained for all f values ranging from 0.25 to 0.40. For D values larger than 220 nm an etch depth of about 2.5 μm was achieved. However, for smaller D we observed a decrease of the hole depth with decreasing D. In other words, the etch rate for smaller holes lags behind that for bigger holes. This lag effect can have several origins: 1) ion shadowing, i.e., the screening of the ion beam by the mask edge; 2) deflection of the ions due to mask charging; and 3) redeposition of the etch products on the hole walls. At the present time, it is difficult to identify which of these mechanisms is dominant. These factors also affect the shape of the etched holes, often resulting in nonvertical walls (see Fig. 6). Moreover, we observed a slight "bending" toward the hole bottom on most of the etched PCs. The bending occurs in the same direction in the case of the PC structure shown in Fig. 6 while other PC structures etched with the same process show different orientation from one hole to another. The mechanisms responsible for this bending are not yet well understood.

C. PC Structure Layouts

The layout of simple PC slabs is shown in Fig. 7(a). For both samples A and B, ΓM and ΓK oriented structures were fabricated with $a =$ 240–500 nm and $\Delta a = 20$ nm. D values were

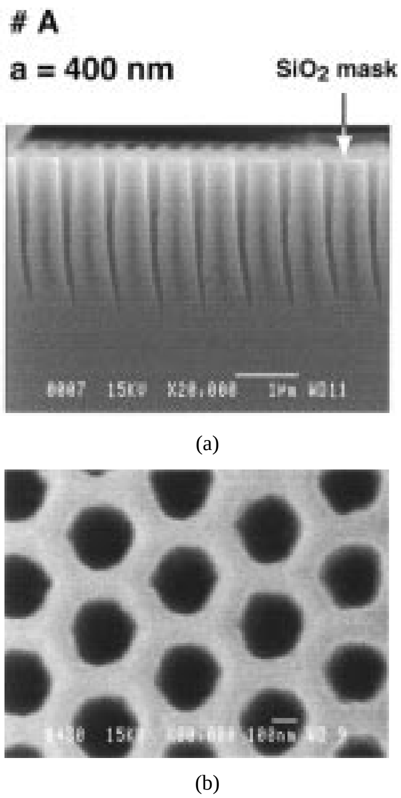

Fig. 5. (a) Edge and (b) top-view SEMs of a PC structure with the same f value as sample A and $a = 400$ nm. The images were taken before the removal of the SiO_2 etch mask.

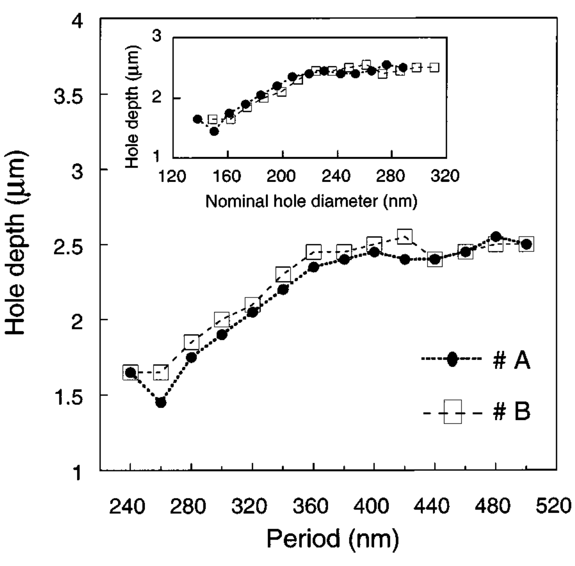

Fig. 6. Measured hole depth of each PC structure of period a for sample A (full circles) and B (open squares) after 20 min of etching with Ar/Cl_2 chemically assisted ion beam etching. The dependence on the nominal hole diameter value $D = a \times \sqrt{2f\sqrt{3}/\pi}$ is presented in the inset for both samples.

chosen in order to keep f constant for each a belonging to the same sample. 30-μm-long PC slabs were fabricated with three different thicknesses: 4, 8, and 10 rows. We note that a single ΓK row is actually made of two different atomic planes [see Fig. 7(a)]. The top-view SEM of a PC test structure with the

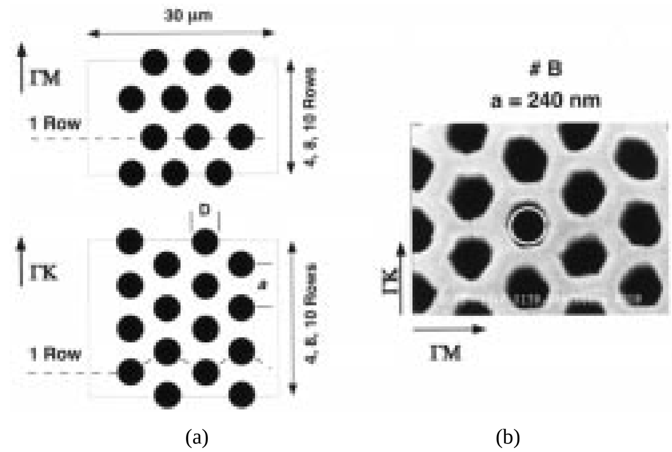

Fig. 7. (a) Sketch of the typical layout of simple PC structures along ΓM and ΓK orientations. Each slab is 30 μm long, 4, 8, or 10 rows thick, and is characterized by the period a (or hole diameter D) value. The air-filling factor f is kept constant for each sample (A and B). Dotted lines show the single "atomic" plane for both orientations. (b) Top-view SEM of a PC slab with the same f value as sample B and $a = 240$ nm. The white circle shows what should be the ideal circular shape of the holes.

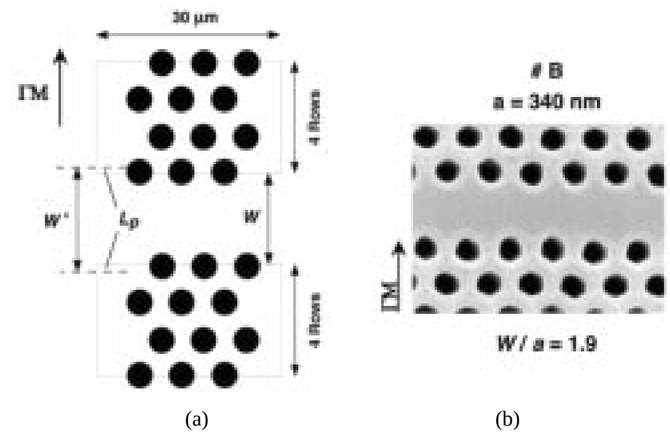

Fig. 8. (a) Sketch of the typical layout of 1-D FP cavities between two ΓM oriented 4-row PC mirrors separated by a spacer W. The cavity structure is 30 μm long. The actual cavity width W' taking into account the finite penetration depth L_p of the field in the mirrors is shown. (b) Top-view SEM of a 1-D cavity structure from sample B with $a = 340$ nm and $W/a = 1.9$.

same f value as sample B and $a = 240$ nm is presented in Fig. 7(b). Due to a slight widening of their width in the ΓK direction, the holes are not circular as expected, but they have an elliptical shape with the principal axis laying along ΓK. The same shape was observed for all f and a values. Since this hole anisotropy was already present in the SiO_2 mask before etching, the origin of the hole "squeezing" has to be found in the e-beam lithography: the direction of the widening corresponds to the scanning direction of the electron beam used to pattern the PMMA resist.

One-dimensional FP cavities were fabricated for both samples using ΓM-oriented PC-based mirrors separated by a spacer W varying from 500 to 1100 nm [see Fig. 8(a)]. PC slabs 30 μm long and 4 rows thick were used as mirrors, with a = 300–480 nm and Δa = 20 nm. The "physical" cavity width W was exactly determined by SEM measurements [see for example Fig. 8(b)]. The following values were found for the normalized width W/a: 1.7, 1.8, 1.9, 2.0, 2.1, and 2.2.

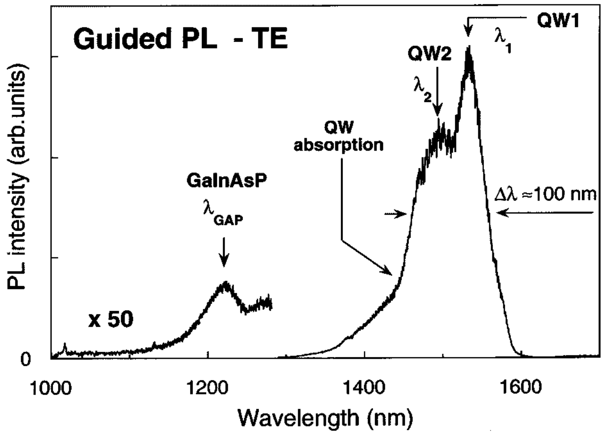

Fig. 9. Typical $I_1(\lambda)$ reference spectrum: the guided PL signal for TE polarization is collected by placing the excitation spot in an unetched region of the sample at a distance $d = 70$ μm from the cleaved edge. Arrows indicate the QW1 and QW2 contributions from the two GaInAsP QWs and the sharp low-wavelength absorption edge due to the QW reabsorption inside the guide. The low-intensity PL emission at λ_{GAP} from the GaInAsP guide core is evidenced ($\times 50$).

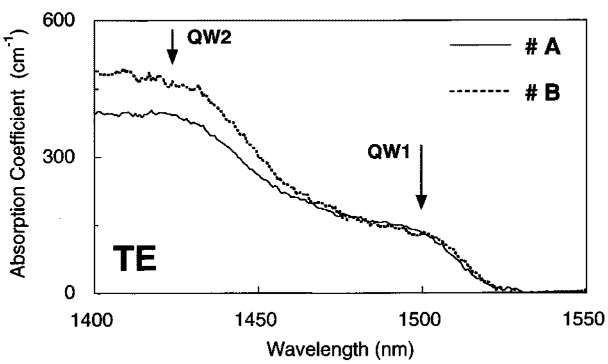

Fig. 10. Measured TE absorption coefficient of the InP/GaInAsP step-index waveguide for sample A (full line) and B (dashed line), respectively. Vertical arrows indicate the QW1 and QW2 contributions from the two GaInAsP QWs.

IV. Experiments and Data Analysis

A. Guided PL Probe Beam

Typical guided PL spectra taken at room temperature with the excitation spot at distance $d = 70$ μm from the cleaved facet are presented in Fig. 9 for the TE polarization. The pump energy density was $\sim$5 kWcm^{-2}. The PL peaks from QW1 and QW2 (see Section III-A) appear at $\lambda_1 = 1530$ nm and $\lambda_2 = 1495$ nm, respectively. The feature evidenced at $\lambda_{GAP} = 1220$ nm is attributed to the $Ga_{0.24}In_{0.76}As_{0.52}P_{0.48}$ layer band-gap emission.

As anticipated in Section II-B, the guided PL spectrum is strongly affected by the QW reabsorption. The absorption coefficient $\alpha(\lambda)$ plotted in Fig. 10 was obtained measuring the bare guided signal $I_1(\lambda, d)$ for different d values between 50 and 100 μm and using a Lambert–Beer-type formula modified to take into account the variation of the collection angle with d [13], i.e.,

$$I_1(\lambda, d) = \frac{A}{d} I_0(\lambda) T_{\mathrm{air}} e^{-\alpha(\lambda) d} \qquad (1)$$

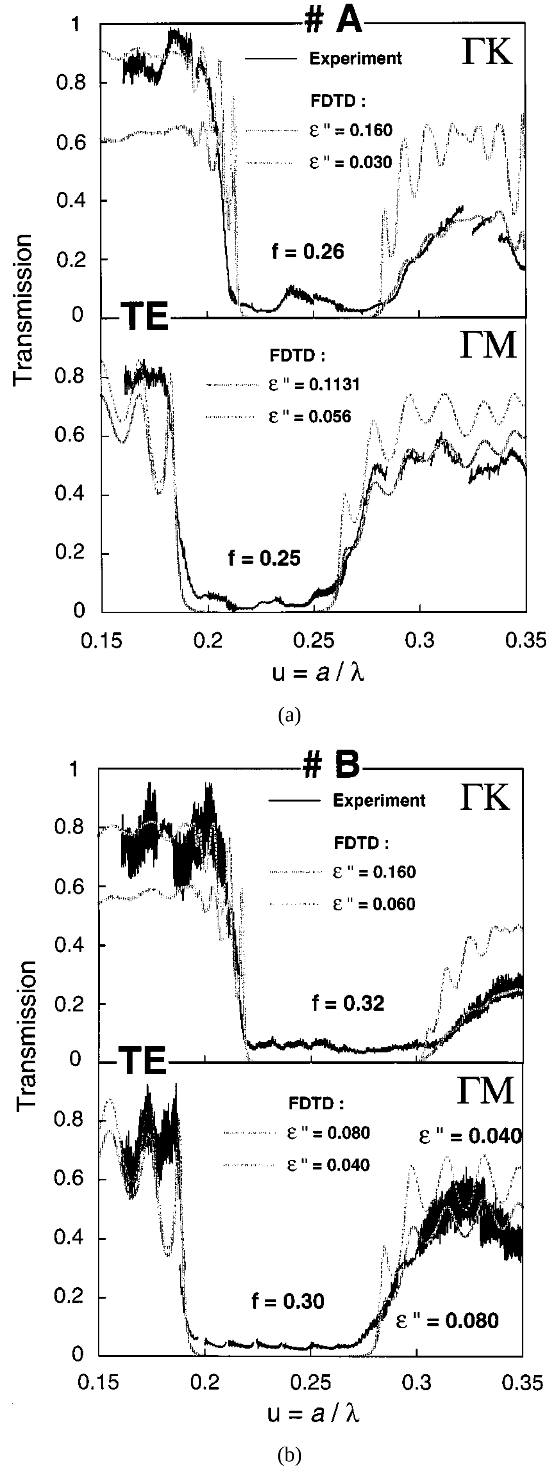

Fig. 11. TE transmission spectra through ΓM and ΓK oriented 10-row PC slabs for samples (a) A and (b) B, respectively. Experimental spectra (black lines) are compared with 2-D finite difference time-domain (FDTD) calculated spectra (gray lines). The effective index value $n_{\mathrm{eff}} = 3.24$ was assumed to account for the vertical confinement on the guided mode. f and the loss parameter ϵ'' were assumed as free parameters yielding the best-fitted values reported in Table I.

where A is a constant, $I_0(\lambda)$ is the total intensity emitted at the excitation point, and T_{air} is the transmission coefficient at the interface with air. The two shoulders centered around the emission wavelengths are due to the TE-polarized electron-heavy-holes recombination in QW1 and QW2, respectively [47].

TABLE I
PC SLABS: PWE AND FDTD BEST-FIT RESULTS

PC slabs (10 rows)		PWE		FDTD		
		Dielectric band edge — Air band edge	f_{PWE}	f_{FDTD}	ε'' (Diel. band)	ε'' (Air band)
# A	ΓM	0.19(0) – 0.26(0)	≈ 0.26	0.25	0.05	0.11
	ΓK	0.21(5) – 0.28(0)		0.26	0.03	0.16
# B	ΓM	0.19(5) – 0.28(5)	≈ 0.32	0.30	0.04	0.08
	ΓK	0.22(0) – 0.30(5)		0.32	0.06	0.16

The strong contribution from QW2 heavily influences the shape of the guided PL spectrum in the low-wavelength region (e.g., the edge at 1440 nm), while due to convolution of the QW1 and QW2 PL peaks an overall spectral window $\Delta\lambda \sim$ 100 nm is obtained. The latter value can be further increased by performing measurements at high pumping power (∼50 kWcm^{-2}). The resulting peak broadening increases the useful spectral window to 130 nm covered by the ILS probe beam. This intrinsic limit could be overcome substituting QWs with quantum dots (QDs) as already done for ILS measurements on GaAs-based structures [12]. Unfortunately, while InP QDs emitting in the visible have been widely studied [48]–[50], the technology of the recent InAs–InP QDs emitting at 1.55 μm is not easily accessible [51], [52], and GaInAsP strain-compensated QWs are at the moment the best available choice [53].

B. Simple PC Slabs

Transmission spectra through 10-row-thick PC slabs along both ΓM and ΓK orientations and for TE polarization are shown in Fig. 11(a) and (b) for samples A and B, respectively. Well-defined stop-gaps appear in the spectra for each sample in both orientations. The energy position of the dielectric and the air band-related transmission edges are reported in Table I. As expected [12], ΓK edges are located at higher energies than the ΓM corresponding ones: due to the higher k value at the Brillouin zone edge, the ΓK stopband is centered at a higher energy than the ΓM stopband but has a similar width. As widely demonstrated by purely 2-D band structure calculations [12], when triangular lattices of air holes in a dielectric matrix are considered, the TE gap width increases with f as well as the dielectric and air band edge energies. In agreement with the choice of $f_A < f_B$ (see Section III-B), sample B spectra present slightly wider bandgaps and blueshifted edges with respect to the corresponding sample A spectra. Interference-like features appear outside the stop-gaps: they are particularly evident in the air-band transmission branches of sample A spectra. These T oscillations originate from interferences between Bloch waves which propagates inside the PC. Due to reflections at the PC boundaries, the Bloch waves achieve round trips inside the slab which finally acts toward them like a thin slab [16]. In the low-energy pass window (i.e., $u = 0.15$–0.20), T reaches values between 80% and 90% for the two samples in both orientations. On the other hand, due to the stonger influence of out-of-plane losses on the air band transmission [12], a lower T level (∼30–60%) is observed in correspondence with the high-energy (i.e., $u \geq 0.30$) pass window. The higher in-plane diffraction efficiency for ΓK than for ΓM [15] lowers T values at the ΓK air band edge with respect to the ΓM one. Finally, an average transmission $T \sim$ 3%–5% is observed inside the gap for both samples. We will discuss in detail the possible origin of this anomalously high T level in Section IV-C. The bumps appearing in the middle of the stop-gap in sample A spectra are to be ascribed to fluctuations in PC fabrication parameters such as f.

Since the TE gap width represents an indirect measure of f, the photonic bandstructure of the triangular lattice of air holes was calculated for different f values and the dielectric and air band edge energy positions were determined as a function of f. A standard 2-D PWE method was used [54]. The effect of the vertical confinement on the light propagating through the PC slabs was taken into account assuming $n = n_{\text{eff}} = 3.24$ for the dielectric matrix. Both the space-dependent dielectric constant and the fields are expanded into a plane-wave basis and inserted into Maxwell's equations. The resulting eigenvalue equation provides the frequencies for different k-values. Since the investigated system is quasi-2-D with a mirror symmetry in the vertical direction, the modes can be separated into TE and TM polarizations. A complete bandgap calculation performed in the framework of a 2-D FDTD model will be illustrated below. However, it is worth noting that, since its simplicity and precision, the PWE method constitutes a fast characterization tool enabling us to determine the effective f value from the position of the band edges. While the energy of the dielectric band edge is roughly independent of f for f values lower than 0.50, the opposite behavior holds for the air band edge. In the latter case, since the electric field is located mostly in the air holes, the energy of the band edge grows rapidly with f [12]. Thus, by fitting the location of the air band edge, the effective f_{PWE} values reported in Table I were deduced. As expected (see Section III-B), f_{PWE}(A) $< f_{\text{PWE}}$(B) while both values fall inside the nominal intervals $f = 0.25$–0.30 and $f = 0.30$–0.35 for samples A and

B, respectively. This confirms the quality of the e-beam/etching procedure and the good control of all fabrication parameters.[1]

The experimental T spectra are compared to theoretical spectra calculated with a 2-D FDTD model (details can be found, for example, in [56]–[60]). As for previous PWE calculations, an index value $n = n_{\text{eff}} = 3.24$ is assumed for the dielectric matrix. Out-of-plane losses are one of the main factors limiting the actual application of 2-D PC slabs into integrated optics and were carefully investigated. As shown in [18], it is possible to translate out-of-plane scattering at the air holes into an effective dissipation and to cast losses into a 2-D calculation with a phenomenological loss parameter (e.g., the imaginary coefficient ϵ''). This phenomenological approach, once validated with full 3D calculations [43], allows a significant reduction in computing efforts and it can be used for PWE as well as for FDTD calculations by introducing a nonvanishing conductivity parameter $\sigma(\lambda) = (c/2\lambda)\epsilon''$ [60]. Finally, in order to absorb the outgoing electromagnetic waves, Berenger's perfectly matched layers were used as absorbing boundaries [61]. f and ϵ'' were chosen as free parameters of the fit. The best-fit curves are reported in Fig. 11, while in Table I the best-fit values for f (f_{FDTD}) and ϵ'' are listed.

If the dielectric and air pass windows are considered, the quality of the fit is good: the calculated curves reproduce well both the dielectric and the air band edges as well as their "fine structure." On the contrary, a significant discrepancy appears within the photonic bandgap: experimental data give $T \sim$ 3–5%, while the best-fit spectra show T values as low as 10^{-4}–10^{-6}. The origin of this discrepancy will be discussed in Section IV-C. The f_{FDTD} and the f_{PWE} values agree. Both for samples A and sample B, $f_{\text{FDTD}}(\Gamma\text{K}) > f_{\text{FDTD}}(\Gamma\text{M})$. This can be understood if the hole morphology is taken into account. As shown in Fig. 7, the top base of the conical holes is slightly elliptical with its principal axis always oriented in the ΓK direction. Therefore, the effective f value is different for ΓM and ΓK directions. Beams impinging on ΓK-oriented PC slabs feel a total volume of air higher than that encountered by light travelling in the ΓM direction.

The ϵ'' values deduced for sample A well agree with the corresponding values obtained for sample B. As already shown by the SEM analysis discussed in Section III-B, that indicates that the hole morphology is similar for both f values and a good uniformity and reproducibility has been achieved in the fabrication procedure for f values ranging from 0.25 to 0.35. However, different ϵ'' values had to be used in order to fit either the dielectric ($\epsilon'' = 0.045 \pm 0.015$) or the air ($\epsilon'' = 0.12 \pm 0.04$) T band edge. An analytic expression for ϵ'' was deduced in [18] using *separability* arguments and a perturbative approach. Even though in further works [42]–[44] the authors have pointed out the necessity of going beyond some assumptions of [18], different 2-D calculations [19] have validated the qualitative behavior of ϵ'' [18]:

$$\epsilon'' \approx \frac{\pi^2}{6} \frac{V}{(\lambda/2n_{\text{core}})^3} \frac{(\Delta\epsilon)^2}{n_{\text{core}}^2} \eta\Gamma_1$$

$$= \frac{2\pi^2\sqrt{3}}{3} \frac{h_{\text{core}}}{\lambda/n_{\text{core}}} (u^2 f)(\Delta\epsilon)^2 \eta\Gamma_1 \tag{2}$$

where $\Delta\epsilon$ is the vertical waveguide index contrast, $V = (\pi/4)D^2\ h_{\text{core}}$ is the hole volume intersected by the guide core, η is the extraction efficiency for a dipole situated in the core, and Γ_1 is the confinement factor in the core. In the lithographic tuning approach, high energy contributions to the spectra are obtained keeping f and λ constant while increasing the period a and the hole diameter D. Therefore, according to (2), while increasing u, increasing ϵ'' values have to be used to fit the experimental spectra. The same argument applies with the hole morphology to explain the discrepancy between the ΓM and ΓK best-fit ϵ'' values. The slightly elliptical hole shape oriented along ΓK results in an anisotropic distribution of the volume V and, according to (2), implies that $\epsilon''(\Gamma\text{K}) > \epsilon''(\Gamma\text{M})$.

Following [42]–[44] and assuming losses from material absorption and fabrication fluctuations (e.g., surface roughness) to be negligible contributions [12], [39], the loss parameter ϵ'' can be written as the sum of two terms, i.e.,

$$\epsilon'' = \epsilon''_{\text{int}} + \epsilon''_{\text{hole}} \tag{3}$$

where ϵ''_{int} accounts for *intrinsic* losses corresponding to the ideal case of infinitely deep holes, while ϵ''_{hole} contains contributions both from the finite etch depth and from the hole shape [44]. Two main sources can be identified for ϵ''_{int}: first, the modal mismatch between the confined mode propagating in the bare waveguide and the Bloch mode travelling in the patterned region (see, for example, [62]). On the other hand, the use of vertical waveguiding heterostructures with low refractive index contrast implies that the PC Bloch modes lie above the light line of the cladding layer and are intrinsically lossy [63]–[65]. Radiation is scattered toward the substrate due both to the finite hole etch depth z_0 [43] and to the conical shape of the holes in the bottom cladding layer [44]. It is worth noticing that ϵ''_{int} is an intrinsic property of these types of PC structure and sets the *minimum* value of losses that can be expected in such structures. From the ϵ''_{int} data obtained in [43] for GaAs-based systems (with higher index contrast and smaller hole diameter) the value $\epsilon''_{\text{int}} = 0.015 \pm 0.005$ can be deduced for these InP-based structures. It is then interesting to evaluate the contribution of ϵ''_{hole} from measurements. As mentioned above, the air band is more sensitive to scattering at the air holes than the dielectric one and, since $\epsilon''(\text{air band}) > \epsilon''(\text{diel. band})$, $\epsilon''(\text{air band})$ sets the upper limit for losses. Therefore, we limited our analysis to the air band, i.e., to PC slabs with $a \geq 380$ nm. From the ϵ''(air band) data reported in Table I, the average value $\epsilon'' = 0.12 \pm 0.04$ can be assumed for both samples, yielding $\epsilon''_{\text{hole}} = 0.105 \pm 0.045$.

The obtained ϵ''_{hole} value can be analyzed using the loss model proposed in [44] to separate contributions from hole depth and shape. For this purpose, we consider PC slabs with $a = 400$ nm. The cylindro-conical hole shape revealed by the SEMs (see Fig. 5) is modeled assuming that the conical part is located entirely in the bottom cladding, while the hole is cylindrical in the top cladding and in the core. The total hole depth is $z_0 \leq 2.45$ μm (see Fig. 6) and the cone base diameter

[1]Note that, for the same gap width, a 2-D calculation results in a slightly higher f value than that provided by a full 3-D model [55].

is $D \sim 215$ nm for both samples. Benisty *et al.* demonstrated in [43] that, for perfectly cylindrical holes, if the exponentially decaying profile $\zeta(z) = A\exp(Kz)$ is assumed in the bottom cladding, losses due to the finite hole depth can be expressed as

$$\epsilon''_{\mathrm{hole}} = B\Gamma(z) \tag{4}$$

where B is a function of the hole diameter and of the vertical index profile [43], [44], while $\Gamma(z_0)$ is the partial confinement factor, i.e., the overlap integral of the squared field profile $\zeta^2(z)$ with the missing air column region. Moreover, one can define an effective depth z_{eff} of an equivalent cylindrical hole giving rise to the same amount of losses of a cylindro-conical hole [44]. z_{eff} can be written as an analytical function of $K = (2\pi/\lambda)\sqrt{n_{\mathrm{eff}}^2 - n_{\mathrm{clad}}^2}$ and of the cone slope β in the first L_{decay} (where $L_{\mathrm{decay}} = K^{-1}$), provided that β remains constant until at least z_{eff} [44].

In our case, substituting z_{eff} for z in (4) (where $B = 20$ [44]) gives $z_{\mathrm{eff}} = 1.35$ μm. Following the procedure illustrated in [44], with $K = 3$ $\mu\mathrm{m}^{-1}$, the angle value $\beta = 1.7°$ is calculated from z_{eff}. On the other hand, from the SEM analysis $\beta = 2.5° \pm 0.5°$ is found for both samples. This discrepancy may be explained considering that the actual geometrical shape of the holes is more complex than the adopted model and both hole bending and the fact that the cones already start within the core have been neglected [see Fig. 5(a)]. Nevertheless, when the holes have vertical walls inside the cap+waveguide layer and no bending is present, information on the hole depth and shape can be safely deduced from the analysis of the experimental $\epsilon''_{\mathrm{hole}}$ values and the model turns out to be predictive [44]. For example it is found that the minimum loss limit $\epsilon''_{\mathrm{hole}} = \epsilon''_{\mathrm{int}}$ could be reached for $\beta < 0.5°$, i.e., for holes with almost vertical walls in some L_{decay}s.

C. 1-D FP Cavities

Typical transmission spectra through 1-D FP cavities between 4-row ΓM PC mirrors (see Section III-C) are shown in Fig. 12(a) and (b) for sample A (with $W/a = 1.8$) and sample B (with $W/a = 1.9$), respectively. In agreement with the results for simple 10-row ΓM PC slabs discussed in Section IV-B, the air T band edge lies at $u \sim 0.26$ for sample A and $u \sim 0.28$ for sample B. Due to FP resonances inside the cavity, sharp first-order peaks in transmission appear within the photonic bandgap at $u_{\mathrm{FP}} = 0.227$ and $u_{\mathrm{FP}} = 0.230$ for samples A and B, respectively, while a second-order peak appears at $u = 0.290$ in sample B spectra because of the larger cavity width. The energy location of the first-order FP resonances for all the investigated cavity widths (see Section III-C) is reported in Fig. 13 for both samples.

For comparison, theoretical T spectra were calculated applying the same FDTD method used for the analysis of PC slab T spectra (see Section IV-B). The ΓM values reported in Table I were used for f and ϵ'': $f = 0.25$ and $\epsilon'' = \epsilon''(\mathrm{air}) = 0.1131$ for sample A, while $f = 0.30$ and $\epsilon'' = \epsilon''(\mathrm{air}) = 0.080$ for sample B. With FP cavities, a third free parameter has to be considered: the cavity width. Two values adjacent to the actual W/a value were chosen for simulations: 1.77 and 1.87 for sample A ($W/a = 1.8$); 1.87 and 1.97 for sample B ($W/a = 1.8$). The

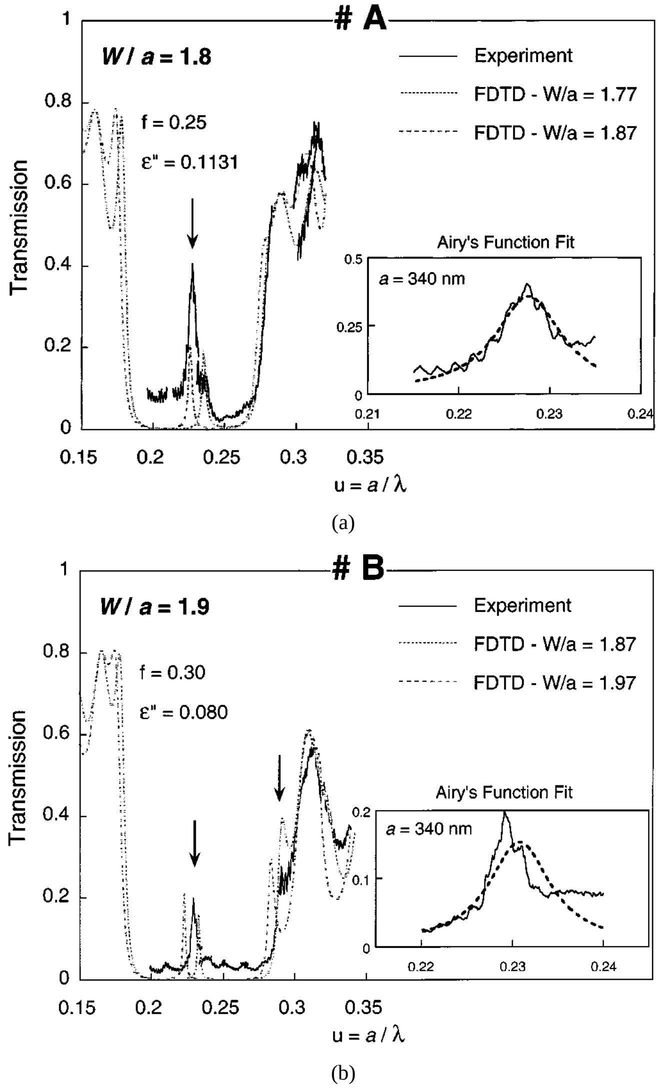

Fig. 12. Transmission spectra through 1-D FP cavities between two ΓM oriented 4-row PC mirrors separated by a spacer W. The case of (a) $W/a = 1.8$ and (b) $W/a = 1.9$ are shown for samples A and B, respectively. Arrows indicate transmission peaks related to first and second order FP resonances. Experimental spectra (black lines) are compared with 2-D FDTD calculated spectra (gray lines). The effective index value $n_{\mathrm{eff}} = 3.24$ was assumed to account for the vertical confinement on the guided mode. The values reported in Tables I and II were used for f, ϵ'' and W/a. The Airy's function best-fit (dashed lines) of the first-order FP peak for $a = 340$ nm is shown in the insets for both samples.

calculated spectra are plotted in Fig. 12. As for simple PC slabs, both the air T band edge and the interference-like features in the high-energy pass window are well reproduced, thus confirming the reliability of the fabrication process: no fluctuations can be observed in PC parameters when different structures (4, 8, or 10 row-thick slabs, 1D FP cavities, etc.) are compared. The energy position of the FP resonances, which depends only on the cavity width (see below) [66], is consistent with calculations.

As for simple PC slabs, FDTD calculated spectra do not agree with experimental T data inside the photonic bandgap. The base transmission level T_{GAP} is still too high and the experimental FP resonances show higher peak transmissions $T_{\max}$ and lower quality factors $Q = \lambda_{\mathrm{FP}}/\Delta\lambda_{\mathrm{FP}}$ (where λ_{FP} and $\Delta\lambda_{\mathrm{FP}}$ are the resonance wavelength and the peak width, respectively) than the simulated ones. Two possibilities can be identified in order to

TABLE II
1-D FP CAVITIES: SINGLE MIRROR OPTICAL PROPERTIES AND CAVITY

	PC Slabs	1D - FP Cavities							
		Airy's function fit					u_{FP}^{-1} (W/a) fit		Q
	T_{GAP} (%) 4 rows a = 340 nm	T (%)	R (%)	L (%)	L_p/a	m	L_p/a	m	
		a = 340 nm ; W/a = 1.8							
# A	23.5 ± 0.5	23.2 ± 0.3	61.8 ± 0.7	15	0.45	4	0.48 ± 0.05	4.0 ± 0.1	24
		a = 340 nm ; W/a = 1.9							
# B	14.5 ± 0.5	14.2 ± 0.4	64.5 ± 1.2	22	0.36	4	0.35 ± 0.15	3.8 ± 0.4	28

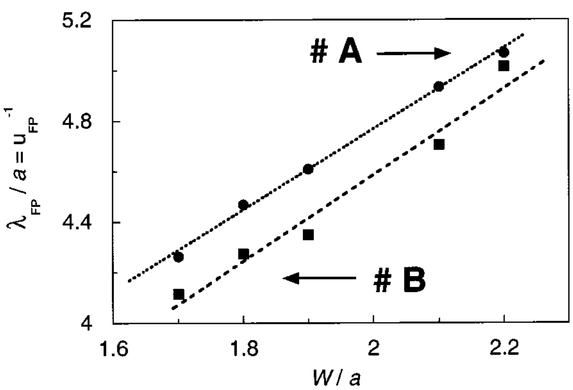

Fig. 13. Normalized resonant wavelength $\lambda_{\rm FP}/a$ of the first-order FP peaks as a function of the normalized cavity width W/a for samples A (circles) and B (squares). The linear best-fit (dotted lines) is also shown.

explain these discrepancies: either high $T_{\rm GAP}$ values have to be ascribed to the existence of some parasitic channels which favor transmission of light through the PC slab, or they are an intrinsic property of these PC structures compatible with the results of FP cavity measurements. In order to clarify this issue, the classical FP resonator theory was applied to these 1-D FP cavities. According to the theory both $T_{\max}$ and Q are functions of T and R values for each mirror [40], [66], so that the optical properties of the PC-like mirrors can be deduced in an indirect way.

FP peaks were best-fitted with the *Airy's formula* [40], [66]

$$T_{\rm FP}(\lambda) = \frac{T^2}{|1 - Re^{2i\varphi}e^{-\alpha W}|^2} \tag{5}$$

where T and R are the transmission and reflection coefficients for a single PC mirror (i.e., for a 4 row-thick ΓM slab), α is the waveguide absorption coefficient (see Fig. 10: $\alpha \sim 100$ cm^{-1} for $\lambda \sim 1500$ nm) and $2\varphi = 4\pi W' n_{\rm eff}/\lambda$ is the normal incidence round-trip phase; $W' = W + 2L_p$ is the actual cavity width taking into account the finite penetration length L_p of the field in each mirror [39]. The physical width W is used to calculate the absorption factor $\exp(\alpha W)$ since α can be considered negligible inside the patterned region. T, R, and W' are fitting parameters. In the insets of Fig. 12(a) and (b) we show both the experimental and the best-fitted spectra for the corresponding 1-D FP cavity structures with $a = 340$ nm. The best-fit parameter values are reported in Table II. $T \sim 23\%$ and $T \sim 14\%$ were found for samples A and B, respectively. These values agree with the corresponding $T_{\rm GAP}$ values measured with 4-row ΓM PC slabs with $a = 340$ nm (see Table II). The intrinsic character of high $T_{\rm GAP}$ values is then assessed confirming that inside the stopgap the theoretical model (2-D-FDTD $+\epsilon''$) cannot reproduce R and T for PC slabs and the related optical parameters (e.g., $T_{\max}$ and Q) for FP cavities.

Since $R \sim$ 62–64%, the overall loss level $L = 1 - R - T$ ranges from 15% for sample A to 22% for sample B. While L values are similar to those found for the corresponding GaAs-based structures [12], [14], [15], [39], the T values are unexpectedly high and $R \ll 100\%$. Further e-beam lithography tests with different higher irradiation doses have shown that, in spite of increased f values, deeper holes with better shape can be obtained with a consequent decreasing of T values.

The normalized penetration length L_p/a was deduced from the best-fitted W'/a values. Then, the cavity order [66]

$$m = 2n_{\rm eff}u_{\rm FP}\left(\frac{W}{a} + \frac{2L_p}{a}\right) \tag{6}$$

was calculated inserting the exact values for W/a and $1/u_{\rm FP}$. The deduced L_p/a and m values are listed in Table II. The same parameters can be evaluated in an independent way by fitting the experimental data $u_{\rm FP}^{-1}$ versus W/a with (6) (see Fig. 13). As shown in Table II, both sets of values are in perfect agreement. Finally, knowing m and R [40], [66], cavity Q values were calculated. The relatively low Q values ($Q \sim$ 20–30) agree with the limited reflectivity of the PC mirrors.

An important conclusion can be drawn from the comparison between R and T values obtained inside the stopgap either from the combined analysis of PC slabs and 1-D cavity experimental data, or by means of the theoretical 2-D-FDTD method including a phenomenological dissipation approach. While the ϵ'' model works outside the stopgap, it fails when moving inside the gap. Let us recall that the propagation of light through the PC structure is affected by the finite hole depth in two different ways. First, as mentioned above, light is scattered toward the substrate and this effect is taken into account in the 2-D-FDTD method introducing the loss parameter ϵ''. Then, the guided light "feels" the holes in the PC as a low refractive index region and is pushed below the guiding layer. This phenomenon is reversible and is neglected in a 2-D calculation. For some reasons which have to be further investigated, the first effect dominates when allowed Bloch modes are considered, while the second one is predominant in the stopgap, i.e., with "evanescent" modes. The influence of the second effect is more pronounced in InP-based PCs than in GaAs-based structures probably because of the combination of the lower index contrast in the planar waveguide and the presence of cylindro-conical holes. It is then evident that further theoretical efforts (e.g., 3D FDTD calculations) are necessary in order to model losses inside the stopgap and/or to find easy figures of merit for the fabrication parameters like those obtained in the ϵ'' 2-D model.

Finally, while the minimum loss limit can be easily achieved for light propagating in the PC improving the etching quality (see Section IV-B), bigger technological efforts seem to be necessary to improve PC performance when working inside the stopgap, i.e., in the region of interest for integrated optics device applications. Deeper holes with almost straight walls have to be obtained in order to move toward the theoretical values $T < 1\%$ and $R \approx 100\%$.

V. Conclusion

We have presented first ILS transmission measurements on 2-D PCs etched in GaInAsP/InP slab waveguide structures. The possibility of transferring this powerful approach to the study of InP-based PCs have been clearly demonstrated and validated both qualitatively and quantitatively. This opens the way toward a complete extension into the 1.5-μm spectral range of the experimental and theoretical tools whose potential was already demonstrated in GaAs-based systems at 1.0 μm. Once the same information and the same investigation techniques are available, the transfer of results between the two material systems relies mainly on mastering the PC fabrication at the same level. We have shown that a good knowledge of the main issues (e.g., etch depth, hole shape, etc.) for the optimization of InP-based structures has been achieved. The combination between promising experimental results and good agreement with theory makes these first ILS experiments a promising step toward the design and the fabrication of efficient InP-based quasi-2-D PCs with vertical confinement.

As for optical properties as well as for losses, two different regimes have been identified. When light with wavelengths outside the PBG is considered, out-of-plane losses are the main limiting factor for PC performances. Improvements in the hole shape should allow one to lower the light scattering toward the substrate. On the other hand, the situation becomes more complicated for light with energies within the PBG, where the hole "physical" parameters such as the etch depth and the aspect ratio strongly affect the PC optical properties. In this regime, improvements are needed both in fabrication and in theoretical modeling.

Acknowledgment

The authors from EPFL would like to acknowledge S. Olivier, H. Benisty, and C. Weisbuch from LPMC-Ecole Polytechnique Palaiseau (Paris) for fruitful discussions and expert suggestions in assembling and validating the ILS experimental setup.

References

[1] J. D. Joannopoulos, R. D. Meade, and J. N. Winn, *Molding the Flow of Light*. Princeton, NJ: Princeton Univ. Press, 1995.

[2] E. Yablonovitch, "Inhibited spontaneous emission in solid-state physics and electronics," *Phys. Rev. Lett.*, vol. 58, pp. 2059–2062, 1987.

[3] S. John, "Strong localization of photons in certain disordered dielectric superlattices," *Phys. Rev. Lett.*, vol. 58, pp. 2486–2489, 1987.

[4] M. Boroditsky, R. Vrijen, T. F. Krauss, R. Coccioli, R. Bhat, and E. Yablonovitch, "Spontaneous emission extraction and Purcell enhancement from thin-film 2-D photonic crystals," *J. Lightwave Technol.*, vol. 17, pp. 2096–2112, 1999.

[5] J. D. Joannopoulos, S. Fan, A. Mekis, and S. G. Johnson, "Novelties of light with photonic crystals," in *Photonic Crystals and Light Localization in the 21st Century*, C. M. Soukoulis, Ed. Dordrecht, The Netherlands: Kluwer, 2001, pp. 1–24.

[6] S. Y. Lin, J. G. Fleming, D. L. Hetherington, B. K. Smith, R. Biswas, K. M. Ho, M. M. Sigalas, W. Zubrzycki, S. R. Kutz, and J. Bur, "A three-dimensional photonic crystal operating at infrared wavelengths," *Nature*, vol. 394, pp. 251–253, 1998.

[7] J. G. Fleming and S. Y. Lin, "Three-dimensional photonic crystal with a stop band from 1.35 to 1.95 μm," *Opt. Lett.*, vol. 24, pp. 49–51, 1999.

[8] S. Noda, K. Tomoda, N. Yamamoto, and A. Chutinan, "Full three-dimensional photonic bandgap crystals at near-infrared wavelengths," *Science*, vol. 289, pp. 604–606, 2000.

[9] R. B. Wehrspohn, A. Birner, J. Schilling, F. Mueller, R. Hillebrand, and U. Goesele, "Photonic crystals from macropouros silicon," in *Photonic Crystals and Light Localization in the 21st Century*, C. M. Soukoulis, Ed. Dordrecht, The Netherlands: Kluwer, 2001, pp. 143–153.

[10] M. Notomi, T. Tamamura, T. Kawashima, and S. Kawakami, "Drilled alternating-layer three-dimensional photonic crystals having a full photonic band gap," *Appl. Phys. Lett.*, vol. 77, pp. 4256–4258, 2000.

[11] H. Benisty, S. Olivier, M. Rattier, and C. Weisbuch, "Applications of two-dimensional photonic crystals to semiconductor optoelectronics devices," in *Photonic Crystals and Light Localization in the 21st Century*, C. M. Soukoulis, Ed. Dordrecht, The Netherlands: Kluwer, 2001, pp. 117–127.

[12] H. Benisty, C. Weisbuch, D. Labilloy, M. Rattier, C. J. M. Smith, T. F. Krauss, R. M. De La Rue, R. Houdré, U. Oesterle, and D. Cassagne, "Optical and confinement properties of two-dimensional photonic crystals," *J. Lightwave Technol.*, vol. 17, pp. 2063–2077, 1999.

[13] D. Labilloy, H. Benisty, C. Weisbuch, T. F. Krauss, R. Houdré, and U. Oesterle, "Use of guided spontaneous emission of a semiconductor to probe the optical properties of two-dimensional photonic crystals," *Appl. Phys. Lett.*, vol. 71, pp. 738–740, 1997.

[14] D. Labilloy, H. Benisty, C. Weisbuch, T. F. Krauss, R. M. De La Rue, V. Bardinal, R. Houdré, U. Oesterle, D. Cassagne, and C. Jouanin, "Quantitative measurement of transmission, reflection, and diffraction of two-dimensional photonic bandgap structures at near-infrared wavelengths," *Phys. Rev. Lett.*, vol. 79, pp. 4147–4150, 1997.

[15] D. Labilloy, H. Benisty, C. Weisbuch, T. F. Krauss, D. Cassagne, C. Jouanin, R. Houdré, U. Oesterle, and V. Bardinal, "Diffraction efficiency and guided light control by two-dimensional photonic-bandgap lattices," *IEEE J. Quantum Electron.*, vol. 35, pp. 1045–1052, 1999.

[16] D. Labilloy, H. Benisty, C. Weisbuch, C. J. M. Smith, T. F. Krauss, R. Houdré, and U. Oesterle, "Finely resolved transmission spectra and band structure of two-dimensional photonic crystals using emission from InAs quantum dots," *Phys. Rev. B*, vol. 59, pp. 1649–1652, 1999.

[17] T. F. Krauss, R. M. De La Rue, and S. Brand, "Two-dimensional photonic-bandgap structures operating at near-infrared wavelengths," *Nature*, vol. 383, pp. 699–702, 1996.

[18] H. Benisty, D. Labilloy, C. Weisbuch, C. J. M. Smith, T. F. Krauss, D. Cassagne, A. Béraud, and C. Jouanin, "Radiation losses of waveguide-based two-dimensional photonic crystals: Positive role of the substrate," *Appl. Phys. Lett.*, vol. 76, pp. 532–534, 2000.

[19] W. Bogaerts, P. Bienstman, D. Taillaert, R. Baets, and D. De Zutter, "Out-of-plane scattering in photonic crystal slabs," *IEEE Photon. Technol. Lett.*, vol. 13, pp. 565–567, 2001.

[20] S. Fan and J. D. Joannopoulos, "Photonic crystals: Toward large-scale integration of optical and optoelectronic circuits," *Opt. Photon. News*, vol. 11, pp. 28–33, 2000.

[21] A. Sharkawy, S. Shi, and D. Prather, "Multichannel wavelength division multiplexing with photonic crystals," *Appl. Opt.*, vol. 40, pp. 2247–2252, 2001.

[22] T. Baba, "Photonic crystals and microdisk cavities based on GaInAsP–InP system," *IEEE J. Select. Topics Quantum Electron.*, vol. 3, pp. 808–830, 1997.

[23] T. Baba, K. Inoshita, H. Tanaka, J. Yonekura, M. Ariga, A. Matsutani, T. Miyamoto, F. Koyama, and K. Iga, "Strong enhancement of light extraction efficiency in GaInAsP 2-D-arranged microcolumns," *J. Lightwave Technol.*, vol. 17, pp. 2113–2120, 1999.

[24] T. D. Happ, A. Markard, M. Kamp, J.-L. Gentner, and A. Forchel, "In–P based short cavity lasers with 2D photonic crystal mirror," *Electron. Lett.*, vol. 37, pp. 428–429, 2001.

[25] O. J. Painter, A. Husain, A. Sherer, J. D. O'Brien, I. Kim, and P. D. Dapkus, "Room temperature photonic crystal defect lasers at near-infrared wavelengths in InGaAsP," *J. Lightwave Technol.*, vol. 17, pp. 2082–2088, 1999.

[26] O. J. Painter, R. K. Lee, A. Yariv, A. Sherer, J. D. O'Brien, P. D. Dapkus, and I. Kim, "Two-dimensional photonic bandgap defect mode laser," *Science*, vol. 284, pp. 1819–1824, 1999.

[27] O. J. Painter, A. Husain, A. Sherer, P. T. Lee, I. Kim, J. D. O'Brien, and P. D. Dapkus, "Lithographic tuning of a two-dimensional photonic crystal laser array," *IEEE Photon. Technol. Lett.*, vol. 12, pp. 1126–1128, 2000.

[28] C. Monat, C. Seassal, X. Letartre, P. Viktorovitch, P. Regreny, M. Gendry, P. Rojo-Romeo, G. Hollinger, E. Jalaguier, S. Pocas, and B. Aspar, "InP 2D photonic crystal microlasers on silicon wafer: Room temperature operation at 1.55 μm," *Electron. Lett.*, vol. 37, pp. 764–766, 2001.

[29] J.-K. Hwang, H.-Y. Ryu, D.-S. Song, I.-Y. Han, H.-W. Song, H.-K. Park, Y.-H. Lee, and D.-H. Jang, "Room-temperature triangular-lattice two-dimensional photonic band gap lasers operating at 1.54 μm," *Appl. Phys. Lett.*, vol. 76, pp. 2982–2984, 2000.

[30] T. Baba, N. Fukuya, and J. Yonekura, "Observation of light propagation in photonic crystal waveguides with bends," *Electron. Lett.*, vol. 35, pp. 654–655, 1999.

[31] A. Talneau, L. Le Gouezigou, and N. Bouadma, "Spectrally resolved transmission measurements for quantitative evaluation of photonic crystal guiding structures," in PECS3, St. Andrews, U.K., 2001.

[32] H. Benisty, S. Olivier, C. Weisbuch, M. Agio, M. Qiu, M. Swillo, A. Karlsson, B. Jaskorzinska, J. Moosburger, M. Kamp, A. Forchel, R. Ferrini, R. Houdré, and U. Oesterle, "Models and measurements for the transmission of submicron-width waveguide bends defined in two-dimensional photonic crystals," *IEEE J. Quantum. Electron.*, vol. 38, pp. 766–781, July 2002.

[33] A. Talneau, L. Le Gouezigou, and N. Bouadma, "1.55 μm transmission through planar photonic-crystal straight guides and ultra-short bends on InP substrates," in *CLEO*, Baltimore, MD, 2001, p. 263.

[34] M. Swillo, M. Qiu, M. Mulot, B. Jaskorzynska, S. Anand, A. Talneau, and A. Karlsson, "Characterization and modeling of InP/InGaAsP photonic-crystal waveguides," in *Proc. ECOC'01*, vol. 4, pp. 586–587.

[35] M. Mulot, S. Anand, M. Swillo, M. Qiu, B. Jaskorzynska, and A. Talneau, "Low loss InP-based photonic crystal waveguides etched with Ar/Cl_2 chemical assisted ion beam etching," in *Proc. ECOC'01*, vol. 6, pp. 32–33.

[36] C. J. M. Smith, T. F. Krauss, R. M. De La Rue, D. Labilloy, H. Benisty, C. Weisbuch, U. Oesterle, and R. Houdré, "In-plane microcavity resonators with two-dimensional photonic bandgap mirrors," *Proc. IEE Optoelectron.*, vol. 145, pp. 337–342, 1998.

[37] R. P. Stanley, R. Houdré, U. Oesterle, M. Gailhanou, and M. Ilegems, "Ultra-high finesse microcavity with distributed Bragg reflectors," *Appl. Phys. Lett.*, vol. 65, pp. 1883–1885, 1994.

[38] D. Labilloy, H. Benisty, C. Weisbuch, T. F. Krauss, V. Bardinal, and U. Oesterle, "Demonstration of a cavity mode between two-dimensional photonic-crystal mirrors," *Electron. Lett.*, vol. 33, pp. 1978–1980, 1997.

[39] M. Rattier, H. Benisty, C. J. M. Smith, A. Béraud, D. Cassagne, C. Jouanin, T. F. Krauss, and C. Weisbuch, "Performance of waveguide-based two-dimensional photonic-crystal mirrors studied with Fabry–Pérot resonators," *IEEE J. Quantum Electron.*, vol. 37, pp. 237–243, 2001.

[40] B. E. A. Saleh and M. C. Teich, *Fundamentals of Photonics*. New York: Wiley, 1991.

[41] M. Kamp, M. Emmerling, S. Kuhn, and A. Forchel, "Nanolithography using a 100 kV electron beam lithography system with a Schottky emitter," *J. Vac. Sci. Technol. B*, vol. 17, pp. 86–89, 1999.

[42] Ph. Lalanne and H. Benisty, "Out-of-plane losses of two-dimensional photonic crystals waveguides: Electromagnetic analysis," *J. Appl. Phys.*, vol. 89, pp. 1512–1514, 2001.

[43] H. Benisty, Ph. Lalanne, S. Olivier, M. Rattier, C. Weisbuch, C. J. M. Smith, T. F. Krauss, C. Jouanin, and D. Cassagne, "Finite-depth and intrinsic losses in vertically etched two-dimensional photonic crystals," *Opt. Quantum Electron.*, vol. 34, pp. 205–215, 2002.

[44] R. Ferrini, R. Houdré, H. Benisty, M. Qiu, and J. Moosburger, "Radiation losses in planar photonic crystals: Two-dimensional representation of hole depth and shape by an imaginary dielectric constant," J. Opt. Soc. Amer. B, submitted for publication.

[45] C. Youtsey, R. Grundbacher, R. Panepucci, I. Adesida, and C. Caneau, "Characterization of chemically assisted ion beam etching of InP," *J. Vac. Sci. Technol. B*, vol. 12, pp. 3317–3321, 1994.

[46] M. Mulot, S. Anand, C. F. Carlström, and A. Talneau, "Dry-etching of photonic crystals in InP based materials," Phys. Scripta, submitted for publication.

[47] G. Bastard, *Wave Mechanics Applied to Semiconductor Heterostructures*. Paris, France: Les Editions de Physique, 1992.

[48] H. Pettersson, S. Anand, H. G. Grimmeiss, and L. Samuelson, "Optical properties of strained InP quantum dots in $Ga_{0.5}In_{0.5}P$ studied by space-charge techniques," *Phys. Rev. B*, vol. 53, pp. R10497–R10500, 1996.

[49] M. K. Zundel, P. Specht, K. Eberl, N. Y. Jin-Philipp, and F. Phillipp, "Structural and optical properties of vertically aligned InP quantum dots," *Appl. Phys. Lett.*, vol. 71, pp. 2972–2974, 1997.

[50] H. Fu and A. Zunger, "InP quantum dots: Electronic structure, surface effects, and the redshifted emission," *Phys. Rev. B*, vol. 56, pp. 1496–1508, 1997.

[51] J. F. Carlin, R. Houdré, A. Rudra, and M. Ilegems, "Island formation in ultra-thin InAs/InP quantum wells grown by chemical beam epitaxy," *Appl. Phys. Lett.*, vol. 59, pp. 3018–3020, 1991.

[52] A. Rudra, R. Houdré, J. F. Carlin, and M. Ilegems, "Dynamics of island formation in the growth of InAs/InP quantum wells," *J. Cryst. Growth*, vol. 136, pp. 278–281, 1994.

[53] S. Jochum, E. Kuphal, V. Piataev, and H. Burkhard, "Very high compositional homogeneity of 1.55 μm strain-compensated InGaAs MQW structures by MOVPE under N_2 atmosphere," *J. Cryst. Growth*, vol. 195, pp. 637–643, 1998.

[54] M. Plihal and A. A. Maradudin, "Photonic band structure of two-dimensional systems: The triangular lattice," *Phys. Rev. B*, vol. 44, pp. 8565–8571, 1991.

[55] L. C. Andreani and M. Agio, "Photonic bands and gap maps in a photonic crystal slab," *IEEE J. Quantum Electron*, vol. 38, pp. 891–898, July 2002.

[56] M. Qiu and S. He, "Numerical method for computing defect modes in two-dimensional photonic crystals with dielectric or metallic inclusions," *Phys. Rev. B*, vol. 61, pp. 12 871–12876, 2000.

[57] ——, "A nonorthogonal finite-difference time-domain method for computing the band structure of a two-dimensional photonic crystal with dielectric and metallic inclusions," *J. Appl. Phys.*, vol. 87, pp. 8268–8275, 2000.

[58] ——, "Guided modes in a two-dimensional metallic photonic crystal waveguide," *Phys. Lett. A*, vol. 266, pp. 425–429, 2000.

[59] ——, "FDTD algorithm for computing the off-plane band structure in a two-dimensional photonic crystal with dielectric or metallic inclusions," *Phys. Lett. A*, vol. 278, pp. 348–354, 2001.

[60] M. Qiu, B. Jaskorzynska, M. Swillo, and H. Benisty, "Time-domain 2D modeling of slab-waveguide based photonic-crystal devices in the presence of out-of-plane radiation losses," *Opt. Technol. Lett.*, to be published.

[61] J. P. Berenger, "A perfectly matched layer for the absorption of electromagnetic waves," *J. Comput. Phys.*, vol. 114, pp. 185–200, 1994.

[62] M. Palamaru and Ph. Lalanne, "Photonic crystal waveguides: Out-of-plane losses and adiabatic modal conversion," *Appl. Phys. Lett.*, vol. 78, pp. 1466–1468, 2001.

[63] D. M. Atkin, P. S. J. Russell, T. A. Birks, and P. J. Roberts, "Photonic band structure of guided Bloch modes in high index films fully etched through with periodic microstructure," *J. Mod. Opt.*, vol. 43, pp. 1035–1053, 1996.

[64] S. G. Johnson, S. Fan, P. R. Villeneuve, J. D. Joannopoulos, and L. A. Kolodziejski, "Guided modes in photonic crystal slabs," *Phys. Rev. B*, vol. 60, pp. 5751–5758, 1999.

[65] E. Chow, S. Y. Lin, S. G. Johnson, P. R. Villeneuve, J. D. Joannopoulos, J. R. Wendt, G. A. Vawter, W. Zubrzycki, H. Hou, and A. Alleman, "Three-dimensional control of light in a two-dimensional photonic crystal slab," *Nature*, vol. 407, pp. 983–986, 2000.

[66] M. Born and E. Wolf, *Principles of Optics*. Oxford, U.K.: Pergamon Press, 1980.

Rolando Ferrini received the Diploma degree in physics and the Ph.D. degree in condensed matter physics from the University of Pavia, Pavia, Italy, in 1996 and 1999. His dissertation focused on the optical properties of III–V semiconductors.

From 1991 to 1995, he was student at the Almo Collegio Borromeo, Pavia, Italy. In March 2000, he joined the Institut de Photonique et d'Electronique Quantique at the Ecole Polytechnique Fédérale de Lausanne, Switzerland, where he is Scientific Collaborator in the Semiconductor Device Physics group. He is presently in charge of the group effort on photonic band gap structures within the framework of the EEC-funded project Photonic Crystal Integrated Circuits (PCIC). His current research interests include advanced semiconductor optoelectronic components, in particular two-dimensional photonic crystal structures and their applications to integrated optics. He is the author of more than 20 publications.

David Leuenberger graduated from the Institute of Applied Physics at the University of Bern, Switzerland. He is currently working toward the Ph.D. degree at the Swiss Federal Institute of Technology, Lausanne.

In May 2000 he joined the Institute of Quantum Electronics and Photonics at the Swiss Federal Institute of Technology and started his Ph.D. thesis on photonic crystals. His research interests include mainly modeling and characterization of two-dimensional photonic bandgap structures.

Mikaël Mulot was born in Dax, France, on December 2, 1976. He received the engineering degree from Ecole Centrale Paris, Paris, France, in 1997 and the Masters degree in physics from University of Stuttgart, Stuttgart, Germany, in 1999. His thesis was on high-frequency measurements of complex coupled 1.55-μm DFB lasers.

Subsequently, he worked on optical fiber dosimetry during his internship at the French Atomic Energy Commission. In 2000 he joined the Department of Microelectronics and Information Technology, Division of Material and Semiconductor Physics, Royal Institute of Technology, Kista, Sweden, where he is doing his Ph.D. thesis work on fabrication and characterization of photonic crystals in InP-based materials.

Min Qiu (A'99) received the Ph.D. degree in condensed matter physics from the Zhejiang University, Hangzhou, China, in 1999, and the Ph.D. degree in electromagnetic theory from the Royal Institute of Technology (KTH), Stockholm, Sweden, in 2001.

From 1999 to 2000, he was a Visiting Scientist at the Department of Electromagnetic Theory, Royal Institute of Technology (KTH), Sweden. Then he joined the Department of Microelectronics and Information Technology, at the same university, in 2001, where he is currently an Assistant Professor at the Laboratory of Optics, Photonics and Quantum Electronics. He has published more than 30 international refereed journal papers since 1996. His research interests include photonic crystals, integrated optical circuits, solid state theory, electromagnetic theory, and numerical techniques in electromagnetics.

Dr. Qiu is a member of the Optical Society of America.

Jürgen Moosburger studied physics and mathematics at the University of Würzburg. He is now working toward the Ph.D. degree at the University of Würzburgunder Alfred Forchel. The focus of his thesis lies on the development of fabrication techniques for photonic crystal based patterns on compound semiconductor heterostructures while also investigating and characterizing photonic crystal waveguide based patterns.

He is the author or co-author of ten publications in the field of photonic crystals.

Martin Kamp was born in Lippstadt, Germany, in 1971. He studied physics at the University of Würzburg and spent one year at Stony Brook University, NY, where he received the M.A. degree in 1995. After his return to Würzburg, he started to work on his Ph.D. thesis "Semiconductor lasers with lateral feedback structures."

Currently he is in charge of the Nanodevice group of the Microstructure Laboratory in Würzburg. He is author or co-author of over 30 papers relating to semiconductor lasers or photonic crystals structures. His current research interests include the development of new patterning technologies for semiconductor lasers, complex coupled DFB lasers, photonic crystals, and their application to optoelectronics.

Alfred Forchel received the Ph.D. degree in physics from Stuttgart University, Stuttgart, Germany, for his work on optical investigations of highly excited semiconductors in 1982 and the Dr. habil. degree for studies on "Dimensionality dependent electronic properties of semiconductor structures" in 1988.

From 1993 until 1989 he was in charge of the whole planning of the microstructure laboratory at Stuttgart University. In 1990, he became a Full Professor of Physics at Würzburg University, Würzburg, Germany. In addition to the chair of Technical Physics, A. Forchel is responsible for the Microstructure Laboratory of University. He is the co-author of over 300 papers relating mainly to optoelectronic devices and to optical properties of semiconductor microstructures. Currently the main scientific interests of A. Forchel are related to the development of novel lateral patterning technologies of III–V semiconductors for semiconductor lasers and the optical investigations of low-dimensional photonic systems and electronic structures.

Srinivasan Anand was born in Bangalore, India, on March 4, 1964. He received the B.Sc. and M.Sc. degrees from the University of Mysore, Mysore, India, in 1984 and 1986, respectively, and the Ph.D. degree from the University of Mumbai, Mumbai, India, in 1993. His thesis work was on spectroscopy of DX centers in AlGaAs and pressurized GaAs and was done at the Tata Institute of Fundamental Research, Mumbai.

He was a Post-Doctoral Fellow at the Department of Solid State Physics, Lund University, Lund, Sweden, where he worked on several topics including space charge spectroscopy of quantum dots and Schottky barriers with nanoscale inhomogeneities. In 1997 he joined the Department of Microelectronics and Information Technology, Division of Material and Semiconductor Physics, Royal Institute of Technology, Kista, Sweden, as a Senior Researcher and obtained the title of Docent in 2000. He leads the research activities of the division in the area of semiconductor processing and characterization. His current research activities are on self-organized nanostructures, ion-beam etching methods for III–Vs, fabrication and characterization of photonic crystals in InP-based materials and scanning probe-based high-resolution electrical characterization of semiconductor materials, devices, and processing.

Romuald Houdré received the Ph.D. degree from the Ecole Polytechnique, Paris, France, in 1985 for his work on the photoemission from quantum wells and superlattices under negative electron affinity.

He spent one year as a Post-Doctoral Fellow at the University of Illinois at Urbana-Champaign with Pr. H. Morkoc in the Molecular Beam Epitaxy (MBE) group. He joined Ecole Polytechnique Federale de Lausanne, Switzerland, in 1988 where he is presently in charge of the photonic crystal group effort within the Microcavity Photonics project. His interest includes microcavities, photonic bandgap structures, and MBE. He is the author of 207 publications.